

that is independent of thickness [30]. The effective impedance, on the other hand, is a linear function of thickness in the same thin shell approximation. These two basic facts together indicate that by choosing the material and the thickness, it is possible to achieve a wide range of effective properties, as illustrated in the chart in Figure 1 (motivated by earlier work in [13]). This is the central idea in the present work.

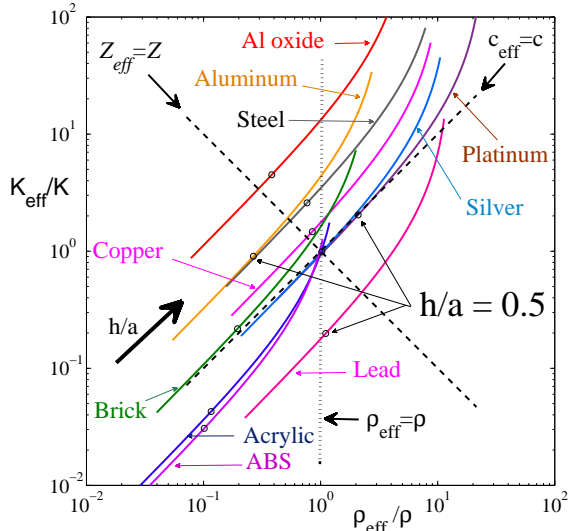


FIG. 1: The effective density ρ_{eff} and bulk modulus K_{eff} of hollow cylindrical shells for ten commonly available materials normalized relative to water, from eq. (4). Each curve shows the properties as a function of the relative thickness to radius ratio $\frac{h}{a}$, from small to large as indicated by the arrow. Circles indicate the values for $\frac{h}{a} = 0.5$. Diagonal dashed lines indicate where the effective acoustic speed and impedance coincide with those of water. (Color online)

The purpose of the present paper is to demonstrate the potential for TA-based GRIN lens design in water using the wide variety of shells available. The transformation acoustics example considered in detail here is the cylindrical-to-plane wave lens discussed by Layman et al. [8] It works by steering waves from a monopole source at the center away from the corners to the faces of the lens. The SC of Ref. [8] is based on constructive multiple scattering from finite embedded elastic materials in a fluid matrix, something previously investigated by Torrent and Sanchez-Dehesa [33]. The GRIN lens device considered here expands the possibilities in

Ref. [33] by increasing the range of achievable properties over those presented by Martin et al. [13].

The cylindrical-to-plane wave lens is designed to increase radiation in specific directions. Enhanced directionality has also been experimentally observed [7] for an acoustic source placed inside a two-dimensional square lattice phononic crystal operating at the band-edge frequency [21]. Highly directional acoustic wave radiation is also possible in 2D PCs at pass band frequencies far away from the band edge states, as shown in simulations of a square lattice of steel cylinders in water [35]. The use of the band structure of a periodic square array to produce directional water wave radiation was proposed by [15], and subsequently demonstrated in experimental measurements on a 6×6 array of surface-breaking cylinders [2] with a monopolar source at the array center. Directional radiation has been demonstrated in air using a non-periodic array of cylinders to produce scattering enhancement in the forward direction [6]. Martin et al. [14, 23] produced acoustic GRIN focusing by changing the lattice constant in a PC with elastic shell elements. Parallel zigzag rigid screens have also been proposed as potential focusing and directional beaming devices [28]. While the spatial filtering device described in this paper uses a fluid matrix, Morval et al. [17] show directional enhancement of a monochromatic acoustic source into a surrounding water medium using a square array of cylinders in a solid matrix; the 2-dimensional quadropolar collimation effect is based on square-shaped equifrequency contours of the phononic crystal [34]. Although the solid matrix has obvious practical advantage, the narrow frequency device of [17] yields decreased amplitude in the preferential directions as compared with the free field radiation. The TA-based device described here does not have these limitations, and shows for the first time as far as we are aware, broadband positive gain in a neutrally buoyant square GRIN lens, with obvious implications for low loss underwater application.

The outline of the paper is as follows. Transformation acoustics and the mapping for the cylinder-to-square lens are described in Section II. Acoustical properties of cylindrical shells are discussed in Section III and the proposed design using available cylindrical tubes is presented. The experimental setup is described and acoustical measurements are discussed in Section IV, with concluding remarks in Section V.

II. CONFORMAL TRANSFORMATION ACOUSTICS

The transformation of a circular region to a square one can be achieved using a conformal change of coordinates. Conformal mapping is a special case of the general theory of transformation acoustics (TA). Usually, in TA one can expect the material properties associated with a spatial transformation to display anisotropy. This could be in the density [5] or the bulk modulus [18], or in both simultaneously [19], but usually something has to become anisotropic. Conformal maps are unique in TA in that they do not require anisotropy. In this case both the inertial [5] and the pentamodal [18] forms of TA converge, and there is no ambiguity or degrees of freedom, a feature that distinguishes TA from its electromagnetic counterpart. At the same time, there is some confusion in the application of TA for conformal mappings, e.g. [22], so we briefly review the correct procedure [20].

We are concerned with a background fluid (water) of density ρ and bulk modulus K in which the acoustic pressure $p(\mathbf{x})$ satisfies

$$\nabla^2 p + \frac{\omega^2}{c^2} p = 0, \quad (1)$$

where $c = \sqrt{K/\rho}$ is the speed of sound and time harmonic dependence $e^{-i\omega t}$ is understood. Under a conformal transformation $z \equiv x + iy \rightarrow z_1(z) \equiv x_1 + iy_1$ the Laplacian ∇^2 in the original variables becomes $|dz/dz_1|^2 |\nabla_1^2|$. If we define the pressure as $p_1(\mathbf{x}_1) = p(\mathbf{x})$ then p_1 satisfies the Helmholtz equation in the mapped coordinates with transformed acoustic speed $c_1 = |z'_1|c$ where $z'_1(z) = dz_1/dz$. This means that the transformed parameters are indeed isotropic, but it does not provide unique expressions for the individual parameters K_1 and ρ_1 , only the combination $K_1/\rho_1 = c_1^2$. The necessary second relation comes from the requirement that the pressure in the transformed fluid arises from a particle displacement field $\mathbf{u}_1(\mathbf{x}_1)$ which satisfies the momentum equation $-\omega^2 \rho_1 \mathbf{u}_1 = -\nabla_1 p_1$ and the pressure constitutive relation $p_1 = -K_1 \nabla_1 \cdot \mathbf{u}_1$. Eliminating \mathbf{u}_1 gives the transformed Helmholtz equation for $p_1(\mathbf{x}_1)$ if and only if ρ_1 is constant, which can be assumed equal to the original density. In summary, the transformed parameters are

$$\rho_1 = \rho, \quad K_1 = |z'_1(z)|^2 K. \quad (2)$$

The lens is based the transformation of a circle of diameter $2b$ into a square of side $2b$, with the precise form of the circle-to-square mapping given in the

Appendix. In particular, we note from eqs. (2) and (A.3) that the mapped value of the bulk modulus associated with the original point (r, θ) in the circle is

$$K_1 = \frac{1.1636 K}{\sqrt{\left(\frac{r}{b}\right)^8 + 2\left(\frac{r}{b}\right)^4 \cos 4\theta + 1}}. \quad (3)$$

Along the principal directions ($\cos 4\theta = 1$) the bulk modulus decreases from the center of the square to a global minimum at the center of the sides. Along the diagonals ($\cos 4\theta = -1$) it increases from its value at the center as it becomes unbounded at the four corners of the square. The overall trend is illustrated in Figure 2.

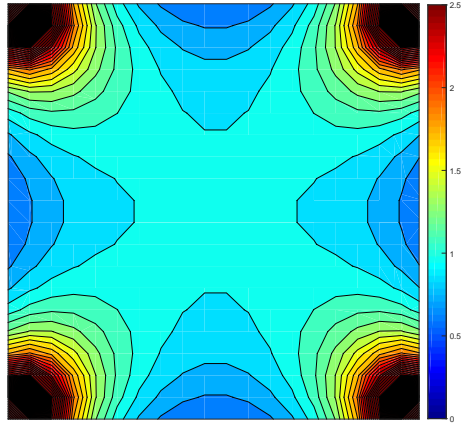


FIG. 2: The bulk modulus distribution K_1/K for the cylindrical-to-square mapping. (Color online)

III. REALIZATION WITH SOLID SHELLS AS METAMATERIAL ELEMENTS

A. Acoustical properties of cylindrical shells

Consider a cylindrical shell of thickness h and outer radius a made of uniform solid with density ρ_s , shear modulus μ_s , and Poisson's ratio ν_s . The interior is air filled, which in the context of water as the ambient medium in the exterior means that we can safely ignore the inertia and stiffness of the interior. The shell's effective density is the average value taken over the circular region of radius a . The effective bulk modulus is the value for which the radial compression of a uniform circular region of fluid

under external pressure is the same as that of the shell under the same pressure, which follows from plane strain elasticity [29, p. 6]. In summary,

$$\begin{aligned}\rho_{\text{eff}} &= (2h/a - (h/a)^2)\rho_s, \\ K_{\text{eff}} &= \mu_s / (2(1 - \nu_s)\rho_s / \rho_{\text{eff}} - 1).\end{aligned}\quad (4)$$

The unit cell of the square array, shown in Figure 3, consists of a solid cylindrical shell surrounded by a complementary region of water. The equivalent

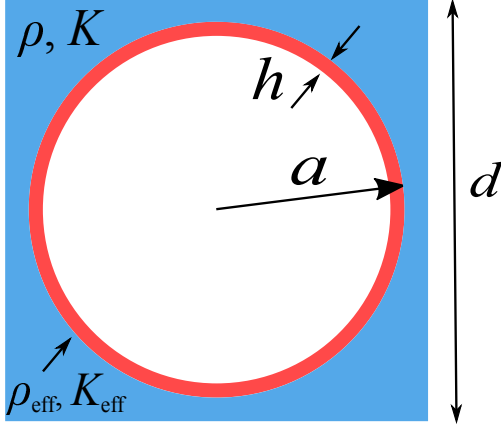


FIG. 3: A square unit cell of a fluid saturated array of shells. (Color online)

density and bulk modulus, ρ_{eq} , K_{eq} , of the unit cell depend on the properties of the surrounding fluid as well as the effective shell properties, according to

$$\rho_{\text{eq}} = (1 - f)\rho + f\rho_{\text{eff}}, \quad (5a)$$

$$K_{\text{eq}} = \left((1 - f)K^{-1} + fK_{\text{eff}}^{-1} \right)^{-1}. \quad (5b)$$

Here $f = \pi a^2 / d^2$ is the shell volume fraction in the unit cell, where d is the cylinder spacing as well as the side length of the unit cell. Since the required density from TA is $\rho_{\text{eq}} = \rho$, it follows that the shell effective density is also constant, $\rho_{\text{eff}} = \rho$. The effective bulk modulus of the shell necessary to achieve the equivalent value from TA is

$$K_{\text{eff}} = \left(K^{-1} + (K_{\text{eq}}^{-1} - K^{-1})f^{-1} \right)^{-1}. \quad (6)$$

The equivalent bulk modulus of the unit cell is significantly affected by the surrounding fluid. With the exception of $n = 0$, all in-plane modes produce no volume change and hence do not change the effective bulk modulus of the unit cell. No significant volume altering modes were observed in the frequency

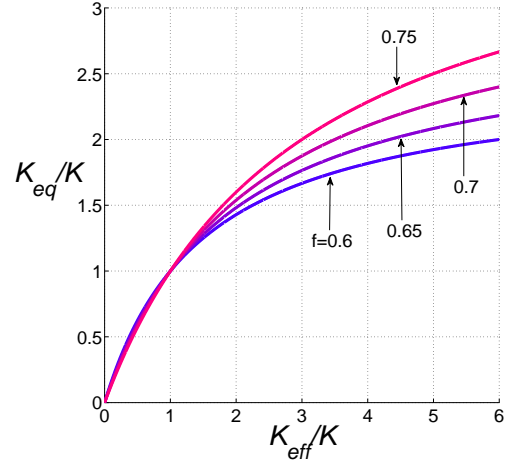


FIG. 4: Equivalent bulk modulus of the unit cell K_{eq} as a function of the effective bulk modulus of the tuned shell K_{eff} for several filling fractions. (Color online)

range considered. Shells of radius $a = 1$ cm with a relatively tight packing of $d = 2.2a$ yields a filling fraction of $f = 0.65$. In this case, in order to have the effective quasi-static bulk modulus of the unit cell $K_{\text{eq}} = 2K$, the effective bulk modulus of the shell-springs-mass system must be $K_{\text{eff}} = 4.33K$, see Figure 4.

The proposed array contains 7 by 7 unit cells of size $d = 2.2a$ with $a = 1$ cm giving a lens side length of $L = 15.4$ cm. The central square element is left empty, requiring 48 cylinders. This was considered the minimal number necessary to provide both a reliable and an accurate gradient index effect. The spacing was chosen to reduce the overall dimension of the lens as much as possible, without making the filling fraction unduly large. Inter-cylinder spacing in the fabricated lens was controlled from the two ends using preformed holders, see Figure 8 below.

Figure 5 shows the discretized values for the equivalent stiffness of each unit cell K_{eq} as determined from Figure 2 by spatial averaging. The effective properties of the shells are obtained from equation (6) with $f = 0.65$, using the required equivalent stiffness of each unit cell K_{eq} in Figure 2. As noted above, this means that effective properties of the shells must be more extreme than those implied by the mapping alone. The effective density of each shell is tuned to water.

2.3	1.24	0.92	0.84	0.92	1.24	2.3
1.24	1.12	0.99	0.95	0.99	1.12	1.24
0.92	0.99	0.99	0.98	0.99	0.99	0.92
0.84	0.95	0.98	0.98	0.98	0.95	0.84
0.92	0.99	0.99	0.98	0.99	0.99	0.92
1.24	1.12	0.99	0.95	0.99	1.12	1.24
2.3	1.24	0.92	0.84	0.92	1.24	2.3

FIG. 5: The spatial distribution of the equivalent bulk modulus K_{eq} in the 7x7 array. The central element is absent (i.e. water) in the constructed design.

B. Design using available cylindrical tubes

The three primary design criteria were: 1) that the shells are readily available, 2) the effective density of each shell approximately matches water and 3) the effect is apparent in the designated frequency range of interest: near 20 to 25 kHz. The shells must be sub-wavelength in dimension. Furthermore all shells are required to have nearly the same outer diameter; therefore, the common outer diameter of 0.5 inches is selected as practical. Fixing this outer dimension leaves two parameters: the shell material and its relative thickness h/a . The range of effective properties as a function of both the shell material and thickness are succinctly summarized in Figure 1.

Several features are apparent from the chart in Figure 1. First, it is clear that the ten materials considered provide a comprehensive range of effective properties. For each material, the effective properties are approximately linear functions of the shell thickness for thin shells ($\frac{h}{a} \ll 1$), with some curvature at larger values of $\frac{h}{a}$. The present design requires shells with effective density equal to that of water, which restricts values of $\frac{h}{a}$ to those near the vertical dotted line. Table I summarizes the properties of available shells which have nearly the same density as water, but varying effective bulk moduli.

Material	OD (in)	h (in)	h/a	ρ_{eff}	K_{eff}	label
PVC	0.54	0.088	0.33	0.71	0.36	1
ABS	0.5	0.125	0.5	0.98	0.52	2
Acrylic	0.5	0.125	0.5	0.89	0.68	3
Polycarbonate	0.5	0.125	0.5	0.90	0.77	4
Brass	0.5	0.14	0.056	0.93	1.63	5
Brass	0.5	0.02	0.08	1.31	2.38	6
Copper	0.625	0.028	0.09	1.50	2.74	7
Aluminum	0.5	0.035	0.14	0.71	2.78	8
Aluminum	0.5	0.049	0.20	0.97	4.13	9
Aluminum	0.5	0.065	0.26	1.24	5.88	10

TABLE I: Readily available shells (i.e. tubes and pipes) with different effective bulk moduli that have effective density close to that of water. All properties are normalized to water.

For the final design we considered only commercially available tubes made from a variety of materials with standard values of radius and thickness. As Figure 1 illustrates, this provides a surprisingly wide range of possible properties, with the added advantage of allowing us to fabricate the lens with minimal effort and cost. Based on the available candidates from Table I we selected nine different shells as shown in Figure 6 for the fabricated lens.

C. Simulations

The total pressure field of the cylindrical-to-square lens made of elastic shells was obtained by numerical computation using COMSOL. Figure 7 shows a simulation for a monopole source of frequency 22 kHz in the center of the lens. Also shown for comparison are the pressure fields for the lens with the unit cells replaced by the effective acoustic medium and the free field radiation of the monopole source.

The simulations indicate that the cylindrical-to-plane wave lens made from the distribution of nine distinct empty shells performs very well as compared the optimal case of each unit cell having the prescribed effective acoustic properties directly from the conformal mapping. It is also evident that the transmission is enhanced in the four principal directions.

The use of empty shells in water acoustics opens up the likelihood of exciting flexural resonances. This is not normally a concern when dealing with isolated shells because the flexural waves are sub-

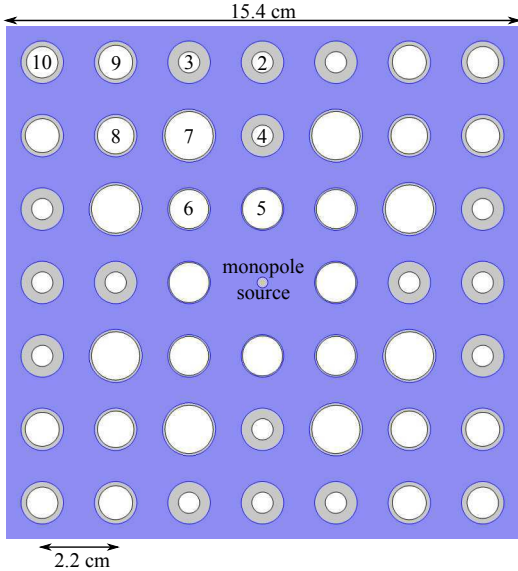


FIG. 6: The 7x7 array of various empty shells. The numbers correspond to the index of each shell shown in Table I. The actual thicknesses of the individual shells are indicated. (Color online)

sonic in speed and hence do not radiate. The present design places the shells in close proximity, leading to the possibility of coherent flexural wave interaction, which can lead to strong scattering. This effect can have positive or negative consequences, depending on one’s immediate goal. In the present situation the shells are of varying thickness and comprised of different materials, with the result that the flexural resonances are spread over many frequencies, which decreases the possibility for coherent interaction. In particular, we note that no such coherent effects were observed in the experiments (see next Section). Related and surprising constructive interference effects resulting from coherent interaction of flexural waves in closely packed arrays of shells in water are described elsewhere [29].

IV. EXPERIMENTAL RESULTS

The device pictured in Figure 8 was fabricated to validate the cylindrical-to-plane wave lens design. The device tested has the cylinder positions, radii, and material properties provided in Figure 6 and Table I. Although the model presented Section III is strictly two-dimensional (2D), which would suggest experimental validation using a 2D water waveguide, the test facilities available to the authors required a

three dimensional (3D) test configuration. Details of the configuration and rationale for their selection are provided here.

The as-tested lens is constructed from cylindrical rods 1 m in height and sealed at either end with urethane end-caps to prevent water intrusion. The cylinders are clamped between 2 cm thick Acrylonitrile-Butadiene-Styrene (ABS) plates using tensioned monofilament. The plates were machined to precisely locate the top and bottom of the cylinders in the positions dictated by the design. Note that an added benefit of the urethane end-caps is that they provide some level of vibration isolation between the end plates and the cylinders. One key challenge to accurately measure the performance predicted in Section III was to minimize the effects of the finite height of the lens and thus observe its 2D response. The associated practical difficulty encountered was in the selection and placement of the appropriate acoustic source. Validation of the lens design implies the need for an axis-symmetric source pressure along the vertical axis in the 3D lens, but no such source was available to the authors nor could one be easily constructed. Acoustic reciprocity, described below, was invoked to resolve this difficulty.

Reciprocity is a fundamental principal of quiescent acoustic media, first fully described for acoustics by Rayleigh [27]; it states that the interchange of source and receiver will lead to the same measured acoustic field if the environment is un-perturbed. Specifically, if one excites acoustic waves at some point, A , then the resulting velocity potential at a second point, B , is the same both in magnitude and in phase, as it would have been at A had B been the source of sound[27]. Applying this principal to the problem at hand, it is possible to replace the axis-symmetric source at the center of the cylindrical-to-plane wave lens with a point receiver and then measure the acoustic field at the center of the lens due to a plane wave incident from a specified radial angle. By varying the angle incidence of the plane wave, it is thus possible to construct the far-field radiation pattern expected from an axis-symmetric source placed at the center of the lens. The only remaining problem is the generation of plane waves at a specified angle of incidence. This is achieved using a spherical wave source located sufficiently far away from the lens such that the phase of the pressure field impinging on the lens aperture has variations less than 1° across the entire frequency band of interest. For the lens geometry and frequencies considered, this can be achieved by at least 10 m separation between the spherical source and the lens.

The experiment was conducted at the Lake Travis

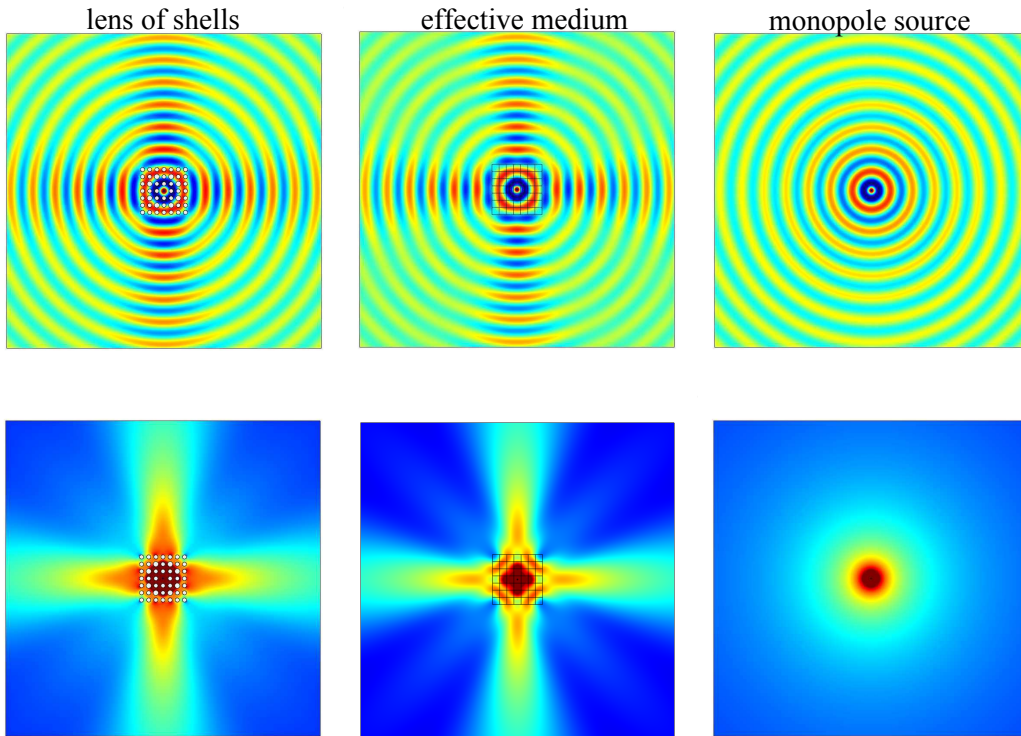


FIG. 7: The left, middle and right columns show the simulated results for the lens of Figure 6, the same square region with the effective acoustic medium from the exact mapping in each unit cell, and the source without the lens, respectively. The top row is the total pressure and the bottom row shows the absolute pressure field for a monopole source at 22 kHz. (Color online)

Test Station (LTTS) of the Applied Research Laboratories (ARL) at The University of Texas at Austin. An A48 hydrophone and associated pre-amplification electronics, which was fabricated and calibrated by the Underwater Sound Reference Division (USRD) of the Naval Undersea Warfare Center (NUWC), was located at the center of the lens. This hydrophone has less than 1 dB of variation across the entire frequency range of interest for this experiment, which was 15–40 kHz. The acoustic source was an omni-directional ITC-1032 fabricated by Channel Technologies Group. The source and lens with internal hydrophone were submerged to a depth of 5.5 m with a separation distance of 10 m. The lens was attached to a column capable of angular rotation through 360°. The source is then driven with 2 ms tone bursts from 15–40 kHz at 2.5 kHz intervals and the time-series voltage output from the hydrophone was collected from 0–360° at approximately 0.5° intervals using a sampling frequency of 512 kHz. This process was then repeated for the hy-

drophone without the lens as a reference and referred to as the bare hydrophone case.

Representative results from the series of experiments conducted on the cylindrical-to-plane wave lens are summarized in Figures 9 and 10. The results were obtained by performing post-processing of the time-series data output from the hydrophone, described next. For each angle and frequency, the steady-state portion of the tone-burst is identified through inspection of the time-domain voltage signal and a time gate is set so that only the steady state portion is considered. The magnitude of the signal at each frequency and angle combination is then found by averaging the magnitude of the complex envelope of the received voltage signal during its steady-state response. This process is carried out for the both measurement configurations (hydrophone in the lens and bare hydrophone). The frequency- and angle-dependent gain is then calculated as $G(f, \theta) = 20 * \log_{10} [|V_{\text{lens}}(f, \theta)| / |V_{\text{no lens}}(f, \theta)|]$. Representative polar plots for $f = 15, 22.5, 25$, and

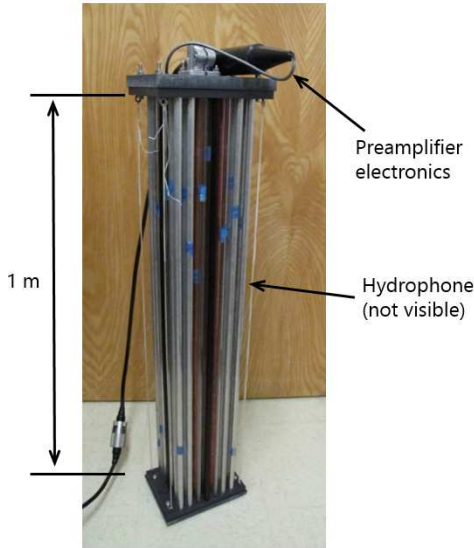


FIG. 8: Constructed device that was tested at Lake Travis Test Station of the Applied Research Laboratories (ARL) at The University of Texas at Austin. The A48 hydrophone is within the lens and the preamplifying electronics are visible. Those electronics are located approximately 1 meter above the lens during the test. The ABS clamping plates and monofilament tensioning elements are visible as are the differing materials of the lens, indicated by changes in cylinder color. (Color online)

40 kHz from experimental data and 2D finite element models are shown in Figure 9. Agreement between model and measurement for the both gain and angular dependence (beam pattern) match very well, with the location of the main lobes observed at 4° , 91° , 176° , and 268° on average across all frequencies inspected (with the exception of the 20 kHz case as described below). Unexpected variations in beam pattern between predicted and measured performance are likely owing to imperfections in the constructed device. One very important observation of this data is the broadband performance of this metamaterial lens. The broadband nature of the response is clearly demonstrated by the results provided in Figure 10, which shows the measured half-power beam width (-3 dB points) and on-axis gain averaged at across all four main lobes. The data clearly show that the as-tested lens provides broadband on-axis gain and beam-widths ranging from approximately $15^\circ - 30^\circ$ for frequencies from 22.5 - 40 kHz, respectively. Finally, it is important to note that the red shaded region in Figures 10 indi-

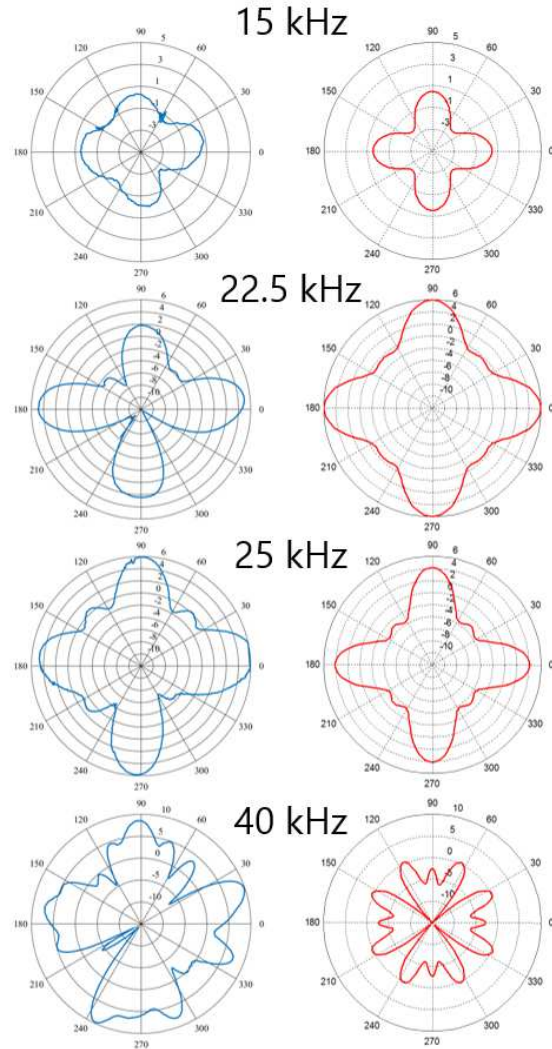


FIG. 9: Angle-dependent gain within the cylindrical-to-plane wave lens at frequencies 15, 22.5, 25, and 40 kHz. The left column presents experimentally obtained angle-dependent gain for a hydrophone within the lens and a plane wave incident from the indicated angle. The right column shows FEM (COMSOL) calculation of far-field radiation beam pattern for a source in the interior of the lens. All plots show gain (radial coordinate) on the same scale and angle range from $0-360^\circ$. (Color online)

cates a regime of flexural tube resonances [29] where the lens behavior was significantly degraded. This experiment provides clear validation of the broadband impedance matched lensing effect provided by hollow cylinder metamaterial elements.

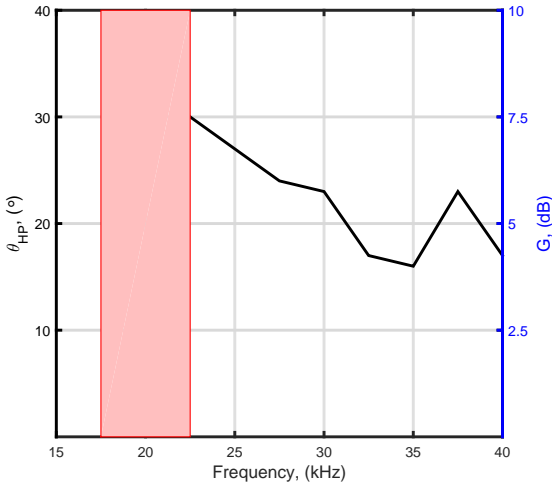


FIG. 10: Half-power beam width (solid line) and average on-axis gain (dot-dash line) of all four lobes of the cylindrical-to-plane wave lens. No beam pattern variations greater than 3 dB were observed for frequencies below 22.5 kHz, and thus no information is provided for $\theta_{HP} < 22.5^\circ$. The shaded region (17.5-22.5 kHz) denotes a flexural tube resonance regime predicted in [29]. Broadband gain and narrow beamwidth is apparent over the entire range of frequencies inspected. (Color online)

V. CONCLUSION

The results of this paper have shown the practical potential of using cylindrical elastic shells as elements in acoustic metamaterial devices. The demonstration test device considered is a cylindrical-to-plane wave structure for which the required element properties are determined from transformation acoustics. The size and material composition of the elements in the square array are chosen based on availability of shells, minimizing fabrication difficulties. The device has the added advantage that is neutrally buoyant by virtue of the transformation acoustics design. Simulations indicated the operating frequency response of the final design would display a surprisingly broadband effect, which is verified in the experimental findings. The underwater measurements show effective conversion of the monopolar source to quadropolar radiation over an octave band (20 to 40 kHz) with positive gain in the desired directions, all despite the minimal number of elements used. These features have been demonstrated for the first time in a water-based acoustic

lens device. Future research will consider other device designs using cylindrical shell passive AMM elements.

Appendix: Circle to square mapping

The Schwartz-Christoffel conformal transformation of the unit disk to a square has been used previously for lens design via transformation optics [26] and transformation acoustics [8]. Here we provide a simpler form of the transformation than that given in [8, 26].

Our objective is a transformation from the plane of the unit circle, defined by the complex variable γ , to the plane containing the mapped square, defined by the complex variable s (for "square").

We first map the interior of the unit circle to the upper half plane of the variable z through a bilinear transformation as $z = i(1 - w)/(1 + w)$ with $w = \gamma e^{i\pi/4}$. The mapping that takes the upper half of the z -plane to the s -plane containing the square is a special case of the more general mapping known for mapping to polygons. Thus, consider $f(z) = A + Bg(z)$ where

$$g(z) = \int_0^z \prod_{i=1}^3 (\zeta - \zeta_i)^{-1/2} d\zeta. \quad (\text{A.1})$$

Taking $\zeta_1 = 0$, $\zeta_2 = 1$, $\zeta_3 = -1$, we find $g(z) = \sqrt{2}F(\sqrt{z+1}; 1/\sqrt{2})$ where F is the incomplete elliptic integral of the first kind. The parameters A and B are found by setting $f(0) \rightarrow 1 - i$, $f(-1) \rightarrow -1 - i$, and using $F(0; \frac{1}{\sqrt{2}}) = 0$, $F(1; \frac{1}{\sqrt{2}}) = K(\frac{1}{\sqrt{2}}) = \frac{1}{4\sqrt{\pi}}\Gamma^2(\frac{1}{4})$, where $K(k)$ is the complete elliptic integral of the first kind and $\Gamma(n)$ is the gamma function. Hence, in terms of the original γ -plane containing the unit circle

$$s(\gamma) = \frac{2}{K(\frac{1}{\sqrt{2}})} F\left(\sqrt{1 + i\frac{1 - \gamma e^{i\pi/4}}{1 + \gamma e^{i\pi/4}}}; \frac{1}{\sqrt{2}}\right) - 1 - i. \quad (\text{A.2})$$

Equation (A.2) and its inverse map the boundary points in the N, S, E, W, NE, NW, SE and SW directions in the circle and square plane to one another.

The density and bulk modulus are functions of the derivative of the mapping function. The derivative of (A.2) is found from $f'(z) = \sqrt{2}/(K(\frac{1}{\sqrt{2}})\sqrt{z(z^2 - 1)})$ and $z'(w) = -2i/(1 + w)^2$, which gives $s'(\gamma)$. Hence, for $\gamma = re^{i\theta}$, $0 \leq \theta < 2\pi$

and $0 \leq r \leq 1$,

$$|s'(re^{i\theta})| = \frac{2}{K(\frac{1}{\sqrt{2}})} (r^8 + 1 + 2r^4 \cos 4\theta)^{-1/4}. \quad (\text{A.3})$$

The inverse mapping from the square, s coordinate, to the circle, γ coordinate is given by eq. (27) of Titovich and Norris [30].

ACKNOWLEDGMENTS

This work was supported by ONR through MURI Grant No. N00014-13-1-0631 and ULI Grant No. N00014-13-1-0417. Many thanks to Dr. Maria Medeiros of ONR (Code 333) and Dr. Stephen O'Regan of NSWCCD (Code 7220).

-
- [1] L.-W. Cai, D. K. Dacol, D. C. Calvo, and G. J. Orris. Acoustical scattering by arrays of cylinders in waveguides. *J. Acoust. Soc. Am.*, 122(3):1340–1351, 2007.
- [2] M. Chekroun, A. Maurel, V. Pagneux, and P. Petitjeans. Directional source of water waves by a crystal of surface-piercing cylinders. *Comptes Rendus Mécanique*, Jul 2015.
- [3] Y. Chen and Z. Ye. Acoustic attenuation by two-dimensional arrays of rigid cylinders. *Phys. Rev. Lett.*, 87(18):184301, 2001.
- [4] A. Climente, D. Torrent, and J. Sánchez-Dehesa. Sound focusing by gradient index sonic lenses. *Appl. Phys. Lett.*, 97:104103, 2010.
- [5] S. A. Cummer and D. Schurig. One path to acoustic cloaking. *New J. Phys.*, 9(3):45+, 2007.
- [6] A. Håkansson, D. Torrent, F. Cervera, and J. Sánchez-Dehesa. Directional acoustic source by scattering acoustical elements. *Appl. Phys. Lett.*, 90(22):224107, 2007.
- [7] M. Ke, Z. Liu, P. Pang, C. Qiu, D. Zhao, S. Peng, J. Shi, and W. Wen. Experimental demonstration of directional acoustic radiation based on two-dimensional phononic crystal band edge states. *Appl. Phys. Lett.*, 90(8):083509, 2007.
- [8] C. N. Layman, T. P. Martin, K. M. Moore, D. C. Calvo, and G. J. Orris. Designing acoustic transformation devices using fluid homogenization of an elastic substructure. *Appl. Phys. Lett.*, 99:163503+, 2011.
- [9] S.-C. S. Lin, T. J. Huang, J.-H. Sun, and T.-T. Wu. Gradient-index phononic crystals. *Phys. Rev. B*, 79:094302, 2009.
- [10] S.-C. S. Lin, B. R. Tittmann, and T. J. Huang. Design of acoustic beam aperture modifier using gradient-index phononic. *J. Appl. Phys.*, 111:123510, 2012.
- [11] S.-C. S. Lin, B. R. Tittmann, J.-H. Sun, T.-T. Wu, and T. J. Huang. Acoustic beamwidth compressor using gradient-index phononic crystals. *J. Phys. D: Appl. Phys.*, 42:185502, 2009.
- [12] T. Martin, M. Nicholas, G. J. Orris, L.-W. Cai, and D. Torrent. Sonic gradient index lens for aqueous applications. *Appl. Phys. Lett.*, 97:113503, 2010.
- [13] T. P. Martin, C. N. Layman, K. M. Moore, and G. J. Orris. Elastic shells with high-contrast material properties as acoustic metamaterial components. *Phys. Rev. B*, 85(16):161103+, 2012.
- [14] T. P. Martin, C. J. Naify, E. A. Skerritt, C. N. Layman, M. Nicholas, D. C. Calvo, G. J. Orris, D. Torrent, and J. Sanchez-Dehesa. Transparent gradient-index lens for underwater sound based on phase advance. *Phys. Rev. Appl.*, 4(3), Sep 2015.
- [15] J. Mei, C. Qiu, J. Shi, and Z. Liu. Enhanced and directional water wave emission by embedded sources. *Wave Motion*, 47(3):131–138, Apr 2010.
- [16] T. Miyashita. Sonic crystals and sonic wave-guides. *Meas. Sci. Technol.*, 16:R47–R63, 2005.
- [17] B. Morvan, A. Tinel, J. O. Vasseur, R. Sainidou, P. Rembert, A.-C. Hladky-Hennion, N. Swintek, and P. A. Deymier. Ultra-directional source of longitudinal acoustic waves based on a two-dimensional solid/solid phononic crystal. *J. Appl. Phys.*, 116(21):214901, Dec 2014.
- [18] A. N. Norris. Acoustic cloaking theory. *Proc. R. Soc. A*, 464:2411–2434, 2008.
- [19] A. N. Norris. Acoustic metafluids. *J. Acoust. Soc. Am.*, 125(2):839–849, 2009.
- [20] A. N. Norris. Comment on “Design of acoustic devices with isotropic material via conformal transformation” [Appl. Phys. Lett. 97, 044101 (2010)]. *Appl. Phys. Lett.*, 100:066101, 2012.
- [21] C. Qiu and Z. Liu. Acoustic directional radiation and enhancement caused by band-edge states of two-dimensional phononic crystals. *Appl. Phys. Lett.*, 89(6):063106, 2006.
- [22] C. Ren, Z. Xiang, and Z. Cen. Design of acoustic devices with isotropic material via conformal transformation. *Appl. Phys. Lett.*, 97(4):044101+, 2010.
- [23] C. A. Rohde, T. P. Martin, M. D. Guild, C. N. Layman, C. J. Naify, M. Nicholas, A. L. Thangawng, D. C. Calvo, and G. J. Orris. Experimental demonstration of underwater acoustic scattering cancellation. *Sci. Rep.*, 5:13175, Aug 2015.
- [24] V. Romero-García, C. Lagarrigue, J.-P. Groby, O. Richoux, and V. Tournat. Tunable acoustic waveguides in periodic arrays made of rigid square-rod scatterers: theory and experimental realization. *J. Phys. D: Appl. Phys.*, 46:305108, 2013.
- [25] J. Sánchez-Pérez, D. Caballero, R. Martínez-Sala, C. Rubio, J. Sánchez-Dehesa, F. Meseguer, J. Linares, and F. Gálvez. Sound attenuation by

- a two-dimensional array of rigid cylinders. *Phys. Rev. Lett.*, 80(24):5325–5328, Jun 1998.
- [26] M. Schmiele, V. S. Varma, C. Rockstuhl, and F. Lederer. Designing optical elements from isotropic materials by using transformation optics. *Phys. Rev. A.*, 81:033837+, 2010.
- [27] J. W. Strutt. Some general theorems relating to vibrations. *Proceedings of the London Mathematical Society*, s1-4(1):357–368, 1871.
- [28] K. Tang, C. Qiu, J. Lu, M. Ke, and Z. Liu. Focusing and directional beaming effects of airborne sound through a planar lens with zigzag slits. *J. Appl. Phys.*, 117(2):024503, Jan 2015.
- [29] A. S. Titovich. *Acoustic and elastic waves in metamaterials for underwater applications*. PhD thesis, Rutgers University, 2015.
- [30] A. S. Titovich and A. N. Norris. Tunable cylindrical shell as an element in acoustic metamaterial. *J. Acoust. Soc. Am.*, 136(4):1601–1609, Oct 2014.
- [31] A. S. Titovich and A. N. Norris. Acoustic scattering from an infinitely long cylindrical shell with an internal mass attached by multiple axisymmetrically distributed stiffeners. *J. Sound. Vib.*, 228:134–153, March 2015.
- [32] D. Torrent, A. Håkansson, F. Cervera, and J. Sánchez-Dehesa. Homogenization of two-dimensional clusters of rigid rods in air. *Phys. Rev. Lett.*, 96:204302, 2006.
- [33] D. Torrent and J. Sánchez-Dehesa. Acoustic metamaterials for new two-dimensional sonic devices. *New J. Phys.*, 9(9):323+, September 2007.
- [34] J. O. Vasseur, B. Morvan, A. Tinel, N. Swintek, A.-C. Hladky-Hennion, and P. A. Deymier. Experimental evidence of zero-angle refraction and acoustic wave-phase control in a two-dimensional solid/solid phononic crystal. *Phys. Rev. B*, 86(13), Oct 2012.
- [35] J. Wen, D. Yu, L. Cai, and X. Wen. Acoustic directional radiation operating at the pass band frequency in two-dimensional phononic crystals. *J. Phys. D: Appl. Phys.*, 42(11):115417, May 2009.